



OPEN ACCESS

EDITED BY

Chen Ling,
Fudan University, China

REVIEWED BY

Daniel Lj Thorek,
Washington University in St. Louis,
United States
Anns Sarnelli,
Scientific Institute of Romagna for the Study
and Treatment of Tumors (IRCCS), Italy
Shuibin Lin,
Sun Yat-Sen University, China

*CORRESPONDENCE

Madjid Soltani

✉ msoltani@uwaterloo.ca

RECEIVED 12 October 2023

ACCEPTED 06 February 2024

PUBLISHED 26 February 2024

CITATION

Piranfar A, Souri M, Rahmim A and Soltani M
(2024) Localized radiotherapy of solid tumors
using radiopharmaceutical loaded implantable
system: insights from a mathematical model.
Front. Oncol. 14:1320371.
doi: 10.3389/fonc.2024.1320371

COPYRIGHT

© 2024 Piranfar, Souri, Rahmim and Soltani.
This is an open-access article distributed under
the terms of the [Creative Commons Attribution
License \(CC BY\)](https://creativecommons.org/licenses/by/4.0/). The use, distribution or
reproduction in other forums is permitted,
provided the original author(s) and the
copyright owner(s) are credited and that the
original publication in this journal is cited, in
accordance with accepted academic
practice. No use, distribution or reproduction
is permitted which does not comply with
these terms.

Localized radiotherapy of solid tumors using radiopharmaceutical loaded implantable system: insights from a mathematical model

Anahita Piranfar¹, Mohammad Souri², Arman Rahmim^{3,4}
and Madjid Soltani^{1,4,5,6,7*}

¹Department of Mechanical Engineering, K. N. Toosi University of Technology, Tehran, Iran,

²Department of NanoBiotechnology, Pasteur Institute of Iran, Tehran, Iran, ³Departments of Radiology and Physics, University of British Columbia, Vancouver, BC, Canada, ⁴Department of Integrative Oncology, BC Cancer Research Institute, Vancouver, BC, Canada, ⁵Department of Electrical and Computer Engineering, University of Waterloo, Waterloo, ON, Canada, ⁶Centre for Biotechnology and Bioengineering (CBB), University of Waterloo, Waterloo, ON, Canada, ⁷Centre for Sustainable Business, International Business University, Toronto, ON, Canada

Introduction: Computational models yield valuable insights into biological interactions not fully elucidated by experimental approaches. This study investigates an innovative spatiotemporal model for simulating the controlled release and dispersion of radiopharmaceutical therapy (RPT) using ¹⁷⁷Lu-PSMA, a prostate-specific membrane antigen (PSMA) targeted radiopharmaceutical, within solid tumors via a dual-release implantable delivery system. Local delivery of anticancer agents presents a strategic approach to mitigate adverse effects while optimizing therapeutic outcomes.

Methods: This study evaluates various factors impacting RPT efficacy, including hypoxia region extension, binding affinity, and initial drug dosage, employing a novel 3-dimensional computational model. Analysis gauges the influence of these factors on radiopharmaceutical agent concentration within the tumor microenvironment. Furthermore, spatial and temporal radiopharmaceutical distribution within both the tumor and surrounding tissue is explored.

Results: Analysis indicates a significantly higher total concentration area under the curve within the tumor region compared to surrounding normal tissue. Moreover, drug distribution exhibits notably superior efficacy compared to the radiation source. Additionally, low microvascular density in extended hypoxia regions enhances drug availability, facilitating improved binding to PSMA receptors and enhancing therapeutic effectiveness. Reductions in the dissociation constant (K_D) lead to heightened binding affinity and increased internalized drug concentration. Evaluation of initial radioactivities (7.1×10^7 , 7.1×10^8 , and 7.1×10^9 [Bq]) indicates that an activity of 7.1×10^8 [Bq] offers a favorable balance between tumor cell elimination and minimal impact on normal tissues.

Discussion: These findings underscore the potential of localized radiopharmaceutical delivery strategies and emphasize the crucial role of released drugs relative to the radiation source (implant) in effective tumor

treatment. Decreasing the proximity of the drug to the microvascular network and enhancing its distribution within the tumor promote a more effective therapeutic outcome. The study furnishes valuable insights for future experimental investigations and clinical trials, aiming to refine medication protocols and minimize reliance on *in vivo* testing.

KEYWORDS

implantable drug delivery system, prostate cancer, ^{177}Lu -PSMA, mathematical model, radiopharmaceutical therapy

1 Introduction

Prostate cancer is a prevalent malignancy globally, ranking second in incidence among all cancers, and responsible for approximately 15% of newly diagnosed tumors in males (1). The primary factor that determines the burden of the disease is its potential for metastasis, which results in substantial morbidity and mortality among patients (2). Despite advancements, challenges persist in managing metastatic prostate cancer, prompting a shift to earlier-stage therapies for improved outcomes. Typically, prostate tumors are treated through radiation therapy or surgery intervention, both of which may result in serious side effects and may not consistently yield favorable outcomes (3, 4). Numerous medical interventions are accessible for the management of patients with recurrent and metastatic prostate cancer, including androgen deprivation therapy, chemotherapy, and immune-based treatments (5). As the progression of malignancy ensues, the effectiveness of conventional therapies tends to diminish, resulting in the development of resistance to hormonal manipulations, increased toxicity, or the acquisition of castration resistance (5–7). As such, the development of innovative therapeutic approaches, particularly in early-stage disease, is of utmost importance. The emergence of novel therapeutic agents such as radiopharmaceuticals holds great promise in transforming the management of prostate cancer.

Radiopharmaceutical therapy (RPT) is a type of targeted therapy that employs radiolabeled molecules to selectively target cancer cells while minimizing harm to healthy tissue (8–10). There are several types of RPT, and radioligand therapy is one of them (6, 11). This type of RPT employs a ligand that is labeled with a radioactive substance to specifically target and deliver radiation to cancerous cells. The target receptor on the tumor cell is the sole site where the radiolabeled ligand is intended to interact. The demise of the cancerous cell is attributed to the DNA impairment instigated by the alpha or beta radiation emanating from the radioactive element conjugated to the ligand (12, 13). The utilization of specific ligands results in the preferential accumulation of radiopharmaceutical agents in tumors as compared to normal tissues. Despite the potential harm to adjacent healthy cells, cancer cells are more susceptible to radiation due to their higher rate of proliferation and less efficient DNA repair mechanisms. Promoting RPT through the utilization of ^{177}Lu -Lutetium-labeled prostate-specific membrane antigen (^{177}Lu -PSMA) targeting agents is a prime

illustration of radioligand treatment in prostate cancer (11, 14). This method may target prostate cancer cells that express the PSMA protein, producing a more potent therapeutic effect (15). An internalization of ^{177}Lu -PSMA is not required since the typical tissue range of ^{177}Lu beta-rays is 0.23 mm, much greater than the cell diameter (16). Radiopharmaceuticals have the potential to be administered intravenously, thereby enabling a comprehensive attack on all tumors in cases where prostate cancer has metastasized (17). Administration of the drug intravenously to patients in the early stages of cancer, prior to metastasis, may result in organ toxicity, particularly to the liver and kidneys (18, 19).

As previously stated, radiopharmaceuticals are typically administered intravenously (20). Owing to the constrained allocation of systemic blood flow directed specifically towards the tumor and high clearance rate in circulation, only a small fraction of the total administered dosage successfully reaches the intended tumor site. The remaining dose is distributed throughout the body healthy tissues, potentially leading to unfavorable side-effects and outcomes (21). Numerous medications, including radiopharmaceuticals, exhibit rapid plasma clearance, leading to relatively short half-lives (20, 22) limiting efficacious delivery.

To overcome such shortcomings, novel approaches including use of nanocapsules (23) may aid in reducing these restrictions. Nevertheless, there exist various biological barriers that have the potential to diminish the therapeutic effectiveness of nanoparticles. Organs such as the kidneys, spleen, and liver, along with resident immune cells, participate in innate processes aimed at eliminating foreign substances (23, 24). Consequently, the process of clearance leads to a reduction in the amount of nanoparticles that are delivered to the tumor. Furthermore, the inefficient Enhanced Permeability and Retention (EPR) effect results in a mere 0.6–0.7% accumulation of the injected dose of nanocapsules in the tumor (25, 26). This low level of accumulation significantly hampers the bioavailability required to effectively suppress tumor growth (27, 28). As a result of the challenges faced in the delivery of pharmaceuticals to the tumor site while minimizing damage to healthy tissues, researchers are exploring innovative methods. The potential of biodegradable implants for tumor treatment before metastatic has garnered significant attention (29). The efficacy of localized therapies can be significantly enhanced by elevating the regional concentration of cytotoxic treatments at the intended sites

(30). This approach can address the limitations of systemic treatment, such as restricted solubility and transport functionality (29, 30). As such, the utilization of intratumoral biodegradable implants for the delivery of (radio)pharmaceutical therapy to the intended site represents a beneficial strategy for the treatment of solid tumors. The combination of intratumoral biodegradable implants and RPT presents a synergistic approach that holds great potential in revolutionizing the field of oncology.

In the present study, a comprehensive 3D computational model is created for the first time to simulate the dispersion and local release of ^{177}Lu -PSMA-617 following the insertion of a dual-release implant into a solid tumor. Understanding the complex bio-drug interactions governing radiopharmaceutical transfer is crucial for deciphering its intricate mechanisms within tissues. Empirically derived models can offer insights into the process, however, achieving a thorough comprehension of the mechanisms governing drug transport and drug-bio interaction over time is a challenging if not insurmountable task. Mathematical and computational models serve as valuable tools for acquiring a comprehensive understanding of the process (31, 32). The utilization of computational models has the potential to reduce the quantity of animal tests, while also decreasing costs and development duration. The utilization of computational models has the potential to forecast the efficacy of drug-loaded implants in solid tumors, thereby enabling researchers and clinicians to enhance implant design and therapeutic response (29, 33).

Current radiopharmaceutical-loaded dual-release implant systems offer several advantages over brachytherapy in the treatment of early-stage prostate tumors. These systems are capable of performing various types of brachytherapy, such as High-dose rate (HDR) implants through burst release, Low-dose rate (LDR) implants through sustained release, and Permanent implants through their biodegradable feature. In contrast to brachytherapy, this technique offers the advantage of biodegradation, thereby eliminating the necessity for removal of the radiation source from the body and providing a less invasive treatment option. Furthermore, the potential for drug leakage from the implant device allows for access to distant areas and the creation of extensive necrotic areas, surpassing the capabilities of brachytherapy. Moreover, the use of radioligands enables internalization by cancer cells, leading to better therapeutic response and irreversible necrosis.

The main goal of this research is to assess the influence of key factors, including hypoxia (as indicated by low microvascular density), on local delivery. Additionally, the study analyzes the impact of the initial amount of ^{177}Lu -PSMA and binding affinity on the absorbed dose within the tumor. The present model takes into account specific tumor microenvironment characteristics, encompassing elements like hypoxia and microvascular density, and incorporates the unique properties of ^{177}Lu -PSMA. These characteristics play a pivotal role in understanding and optimizing an implantable delivery system for localized radiotherapy. By addressing these parameters, the present study contributes to unraveling the complexities of targeted radiopharmaceutical delivery, aiming for more effective and tailored cancer treatment strategies.

2 Methods

In this investigation, the radioligand is loaded into an implant that can be inserted in the center of the tumor tissue. In practical, the implant can be located by a catheter (34). The total amount of substance that is loaded into the implant, the diameter and height of the implant, and the release rate of the drug are the key design factors which can be determined based on tumor size. Drug distribution involves ^{177}Lu -PSMA release in the interstitium and drug association/disassociation with cell surface receptors at K_{ON} and K_{OFF} rate constants (17). The radionuclide decays by physical decay in all stages. Radiopharmaceuticals in the extracellular space can exit through diffusion into the bloodstream or lymphatic vessels. Yet, dysfunctional lymphatic networks in tumors may hinder this process. Ultimately, radiopharmaceuticals bound to receptors enter cells through endocytosis. This work demonstrates concentration exchange between various biophysical spaces using a multi-compartmental approach. An overview of molecular interaction as a paradigm for radiopharmaceutical administration by implant in the tumor and multi-compartmental model are shown in Figure 1. After the release of ^{177}Lu -PSMA from the implant, ^{177}Lu -PSMA reversibly binds to the receptors present on the surface of cells. Subsequently, ligands may be internalized by the cell and endocytosed.

A comprehensive explanation of equations, parameters, and their corresponding values can be found in the Supplementary File. Subsequently, the underlying physics and governing equations are delineated below.

2.1 Implant

In this study, drug release is characterized by two phases: an initial burst release, followed by a sustained release. The flux, representing the quantity of ^{177}Lu -PSMA released across the implant surface with time, is computed as follows (29) (Equation 1):

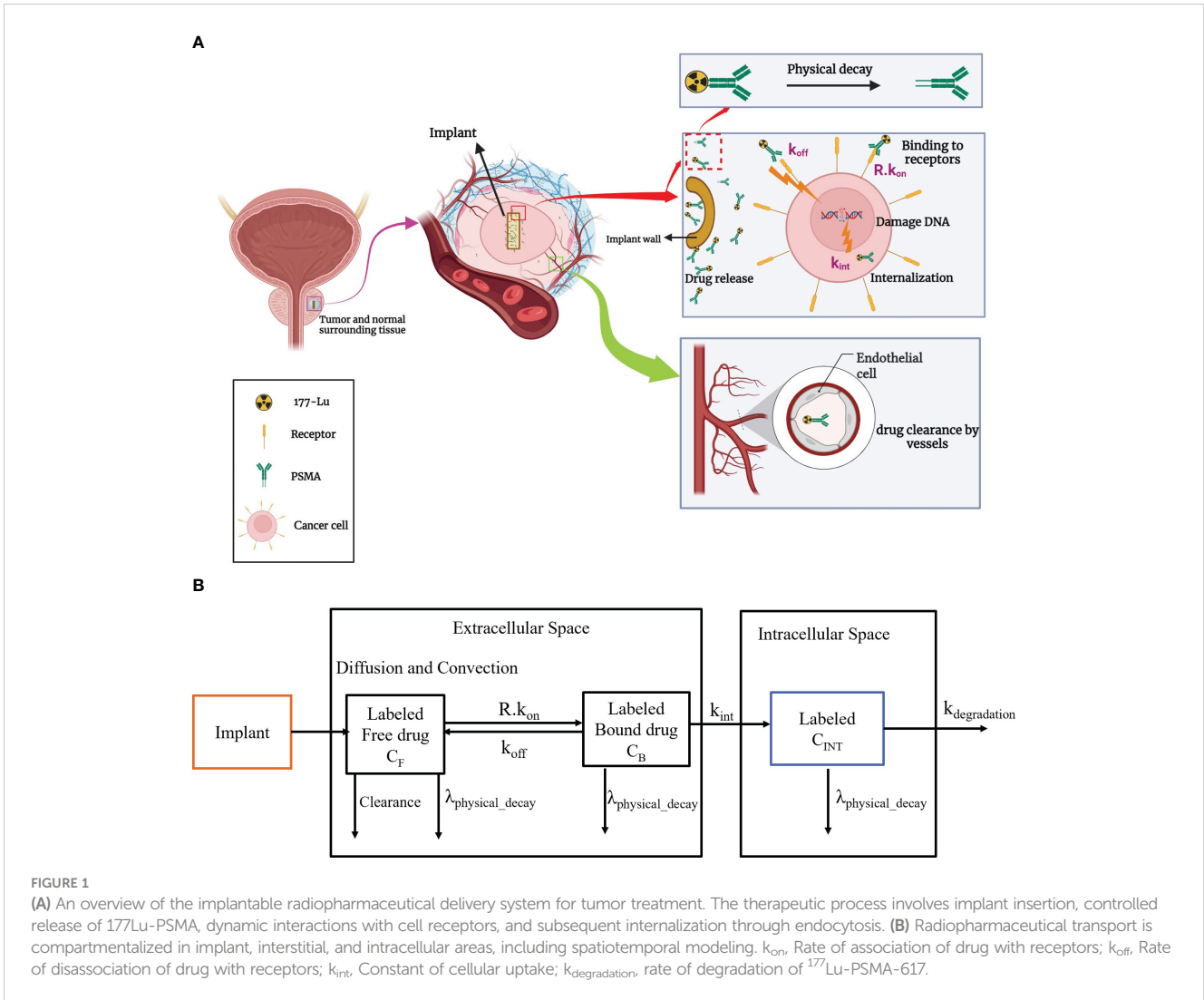
$$R_{177\text{Lu-PSMA}}(t) = \frac{M_0 \cdot w_{\infty}}{A} (f \cdot k_f e^{-k_f t} + (1-f) \cdot k_s e^{-k_s t}) \quad (1)$$

2.2 Fluid flow

Tissue interstitial fluid flow is computed employing Darcy's law (Equation 2), which governs fluid flow through a porous medium, with the inclusion of source and sink terms for biological tissues (Equation 3). The relationship between interstitial fluid pressure (IFP) and interstitial fluid velocity (IFV) within the tissue is established by Darcy's law equation (35, 36). Additionally, transvascular fluid flow is determined using Starling's law.

$$v_i = -\kappa \nabla P_i \quad (2)$$

$$\nabla \cdot v_i = \underbrace{\varphi_B}_{\text{Source term (vessels)}} - \underbrace{\varphi_L}_{\text{Sink term (lymph vessels)}} \quad (3)$$



2.3 ¹⁷⁷Lu-PSMA concentration

The distribution of ¹⁷⁷Lu-PSMA is elucidated utilizing a multi-compartmental model (Figure 1B). A drug that inhibits cancer is released from the implant and diffuses into the surrounding tissue based on convection and diffusion mechanisms (37). Within the interstitial fluid, the transport of radiopharmaceuticals adheres to the Convection-Diffusion-Reaction (CDR) equations (37). Descriptions of the free drug, bound drug, and intracellular drug concentrations are outlined as follows (Equations 4–6):

$$\frac{\partial C_{labeled_F}}{\partial t} = -v \nabla \overline{C_{labeled_F}} + D_{eff} \frac{diffusion}{\nabla^2} C_{labeled_F} - \frac{(R_{max})k_{on} C_{labeled_F}}{\psi} + k_{off} C_B - FC_{labeled} - \lambda_{177} C_{labeled_F} \quad (4)$$

$$\frac{\partial C_B}{\partial t} = \frac{(R_{max})k_{on} C_{labeled_F}}{\psi} - k_{off} C_B - k_{int} C_B - \lambda_{177} C_B \quad (5)$$

$$\frac{\partial C_{int}}{\partial t} = k_{int} C_B - k_{deg} C_{int} - \lambda_{177} C_{int} \quad (6)$$

2.4 Absorbed dose

In radiopharmaceutical therapy, the absorbed dose is the amount of ionizing radiation energy deposited per unit mass of a material (38). To calculate the absorbed for tumor the following equations are used (17, 39, 40) (Equations 7, 8):

$$\dot{D}_i(t) = A_i(t) \cdot S_{i \leftarrow i} = A_0 \cdot a_i(t) \cdot S_{i \leftarrow i} \quad (7)$$

$$D_i(T) = \int_0^T \dot{D}_i(t) dt = A_0 \cdot \tilde{a}_i(T) \cdot S_{i \leftarrow i} \quad (8)$$

2.5 Cell survival probability

Cell survival probability refers to the likelihood that a particular cell will survive following exposure to a specific dose of ionizing

radiation (41). To calculate this probability, linear quadratic models are employed, which consider the absorbed dose (42) (Equation 9).

$$P_S = e^{-\alpha D - \beta D^2} \quad (9)$$

3 Results

3.1 Validation

To ensure the reliability of the present model, qualitative and quantitative comparisons have been made with findings from experimental studies. As the combination of implant and radioligand therapy is introduced for the first time, there are no available results to validate alterations in concentration. Consequently, other influencing factors are scrutinized to evaluate the outcomes and concentration values. In the context of drug delivery within the tumor microenvironment, the intricate interplay of interstitial fluid flow assumes a paramount role in determining therapeutic efficacy. Key parameters governing this flow are IFP and IFV. In numerical models, Darcy's law is commonly employed to describe flow in biological tissues, accounting for tissue porosity. The visual representation in Figure 2 illustrates the spatial

distribution of IFP and IFV. The maximum IFP in the tumor and normal tissue is nearly 1500 and 100 Pa. Furthermore, the IFP in normal tissue is considerably lower than that in tumor. Along the tumor-normal tissue border, a pressure gradient is observed within a confined region. The high leakage of blood microvessels and the dysfunction of lymphatic microvessels contribute to an increase in IFP, which becomes approximately equal to the pressure within the microvessels (44). Significantly, the disparity between tissue pressure and microvascular pressure emerges as a pivotal factor influencing the transvascular exchange of therapeutic agents, with direct implications for drug delivery through convection.

To ensure the validation of the model, a comprehensive comparison was conducted between IFP and IFV obtained from the model and those reported in other relevant studies. Experimental investigations have provided data on the mean spatial pressure in tumor and normal tissues, with reported values ranging from 586 to 4200 [Pa] and -400 to 800 [Pa] (45, 46). The present model's predictions align well with these experimental findings, indicating spatial pressures of 1550 [Pa] in tumor tissue and 65 [Pa] in normal tissue, as depicted in Figure 2. These results not only corroborate the experimental studies but also demonstrate consistency with other numerical investigations (29, 43). Zhan et al. employed a 3D model to examine IFP in prostate tumors and the

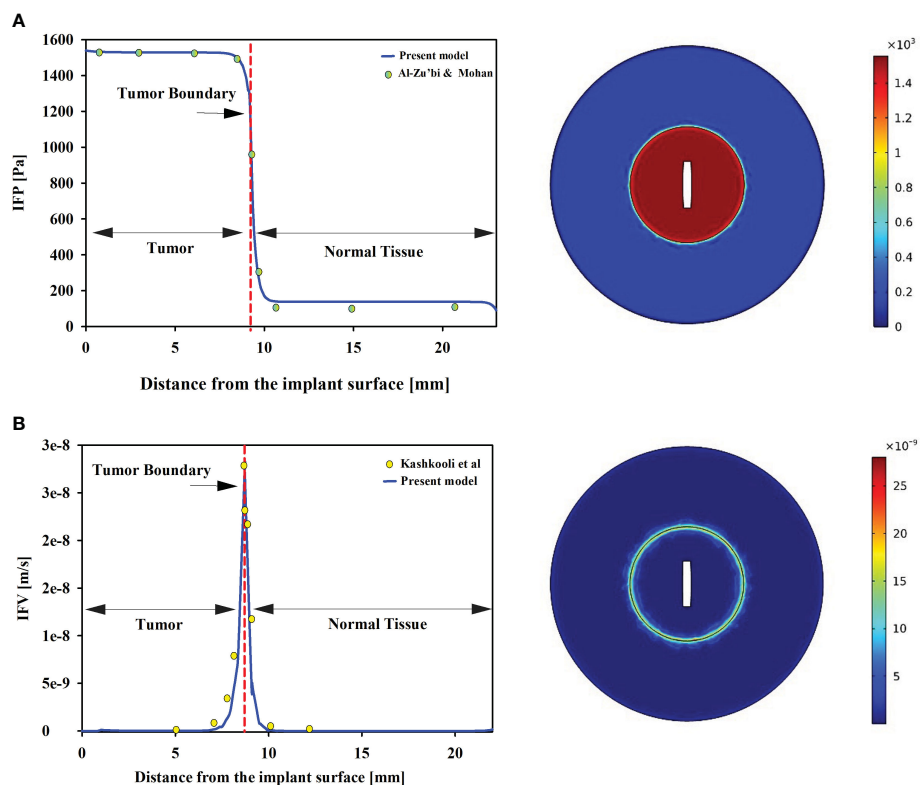


FIGURE 2

(A) IFP in tumor and normal tissue. Tumors exhibit significantly higher IFP compared to normal tissue. Furthermore, uniform distributions of IFP are observed in both tumor and host tissues. Our pressure distribution is validated against Al-Zu'bi and Mohan's numerical models (29). (B) IFV in the tumor and normal tissues. The results show good agreement with Kashkooli et al.'s findings (43). The IFV is also uniform in tumor and normal tissue, with a minimum value, while the maximum value is observed at the tumor and normal tissue border.

adjacent tissue (47). Their study reported a range of IFP values for tumors between 1400-1500 [Pa], while normal tissue exhibited values around 50 [Pa]. Remarkably, the present findings align closely with the outcomes of Zhan et al., underscoring the consistency and reliability of the present results. Additionally, Zhang's investigation (48) also supports the present observations, emphasizing that interstitial fluid pressure in prostate tumors tends to be higher than that in the surrounding tissue, a correlation that resonates with the outcomes of the present study. In contrast to IFP, the IFV exhibits its lowest values within both tumor and normal tissues, while the highest magnitudes occur exclusively at the tumor-normal tissue interface. Remarkably, the present model predicts an IFV on the order of 10^{-8} m/s, which is supported by a previous numerical investigation (49, 50), further enhancing the credibility of the present model's predictions.

3.2 Effect of extension of hypoxia region on the distribution of therapeutic agents

Hypoxia, referring to low density of microvascular networks within the tumor microenvironment, significantly influences the concentration of ^{177}Lu -PSMA-617 in various compartments. The distribution of radiopharmaceutical agents in relation to hypoxic regions is analyzed in Figure 3, shedding light on the impact of hypoxia on ^{177}Lu -PSMA-617 behavior. As depicted in Figure 3A, an increase in tumor hypoxia leads to a rise in the concentration of Free ^{177}Lu -PSMA-617. In the extracellular space, hypoxia causes a reduction in intratumoral blood vessels, hindering the removal of free ^{177}Lu -PSMA-617 from this region (42). Moreover, as illustrated in Figure 3A, it becomes apparent that in the absence of hypoxia, the concentration of free drug in the interstitial space diminishes

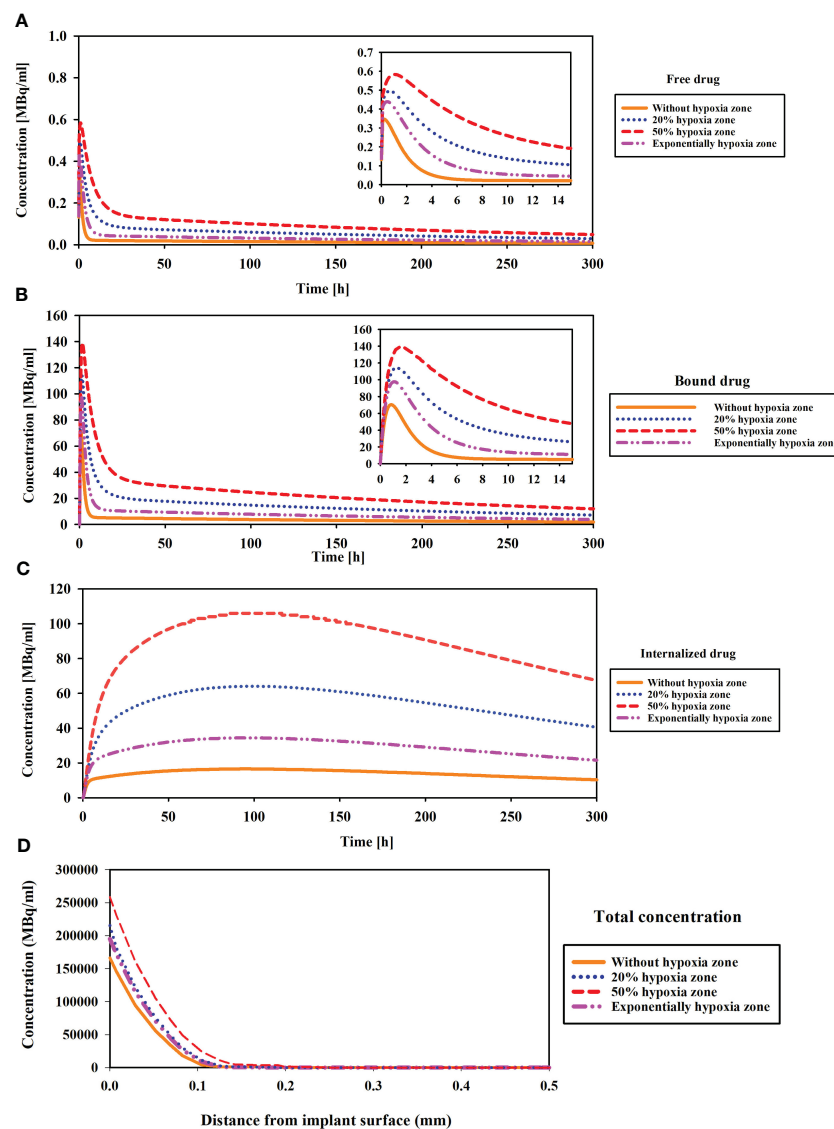


FIGURE 3

Comparison of concentration changes compared to the hypoxia region in different compartments of CDR model. (A) The concentration of released drug from implant (Free drug), (B) Binding drug to receptors, (C) Internalized drug, and (D) The total concentration. Hypoxia with low microvascular density influences ^{177}Lu -PSMA-617 concentration: increased accumulation in extracellular space, enhanced binding to cell surface receptors, elevated internalization within tumor cells and tumor penetration.

and undergoes clearance with a more pronounced slope. This is attributed to the heightened “sink” effect, which is responsible for robustly clearing free drugs from the extracellular space, ultimately resulting in a reduced accumulation of ^{177}Lu -PSMA-617 in this region.

The results demonstrate the peak concentration are observed in the case of 50% hypoxia (Figure 3B). This escalation is attributed to the impact of extension of hypoxic zone and low microvascular density on diminishing the clearance of free ^{177}Lu -PSMA-617, leading to its accumulation and heightened binding to PSMA receptors, consequently elevating the concentrations of bound PSMA. As shown in Figure 3C, when the hypoxia level reaches 50%, the drug concentration rises with a much steeper slope compared to the scenario without hypoxia, ultimately leading to a higher peak concentration. Furthermore, Figure 3D illustrates the total concentration of ^{177}Lu -PSMA versus the distance from the implant surface in the tumor (1 h after implant placement). The 50% hypoxic region is characterized by the highest penetration, attributed to lower vascular density. This condition leads to a reduced clearance of radiopharmaceuticals from the tumor, facilitating deeper penetration of the ^{177}Lu -PSMA.

Finally, in this study, in the presence of 50% hypoxia in the tumor, the TIA increases six-fold compared to the absence of hypoxia (Figure 4). This significant rise in TIA indicates a substantial boost in the overall drug exposure within the tumor microenvironment over time. The heightened TIA highlights the importance of considering hypoxia as a key determinant affecting drug distribution and efficacy in the tumor. Such insights into the impact of hypoxia on drug delivery strategies can pave the way for more effective and precise treatment approaches for prostate cancer patients. When comparing the TIA of the radiation source (implant) and the released drug for the entire tumor, it becomes evident that the radiation source has a significantly inferior performance compared to the released drug. This is due to the fact that the radiation source remains fixed in place and does not reach a substantial portion of the tissue, unlike the released drug.

Therefore, it can be anticipated that the radiation source alone will not generate an effective therapeutic response.

3.3 Effect of binding affinity

The association (k_{on}) and dissociation (k_{off}) rates play a significant role in drug-receptor interactions, impacting the concentration of ^{177}Lu -PSMA-617 and behavior within the tumor microenvironment. The dissociation constant K_D , defined as the ratio of the dissociation rate (k_{off}) to the association rate (k_{on}), characterizes the binding affinity (51, 52). The impact of K_D (1, 0.1 and 0.01 [nM]), derived from various combinations of k_{on} and k_{off} as presented in Table 1, was examined to assess its influence on the time-integrated activity (TIA) of ^{177}Lu -PSMA-617 in the tumor. To investigate the effect of K_D on TIA, a hypoxia-free condition is assumed with an initial ^{177}Lu -PSMA-617 amount of 7.1×10^9 [Bq] in the implant. The results of Table 1 show that with the decrease of K_D , the TIA has increased. This means that when the K_D decreases, the concentration of bound and internalized ^{177}Lu -PSMA-617 in tumors increases over time (Figure 5). Based on Figure 5, a decrease in the dissociation constant K_D for both k_{on} values leads to higher peak concentrations of bound ^{177}Lu -PSMA-617 to receptors and internalized drug. Moreover, a lower K_D implies slower clearance of the radiopharmaceutical agents from the receptors, indicating a stronger and more prolonged binding affinity of PSMA-617 to the receptors on the cell surface. Furthermore, Figure 6 depicts the total concentration profile of ^{177}Lu -PSMA concerning the distance from the implant surface at the one-hour mark following implantation in the tumor. According to Figure 6, when altering k_{off} from 0.1 to 0.001 [1/min] (while maintaining a constant association rate, k_{on} , of 0.1 [L/nmol/min]), the peak total concentration is observed at $k_{\text{off}}=0.001$ [1/min]. This implies that PSMA ligands have more time for entry into the cells under this dissociation rate. The present study's findings align with those reported by Begum et al. (51), who utilized a physiologically based pharmacokinetic (PBPK) model to

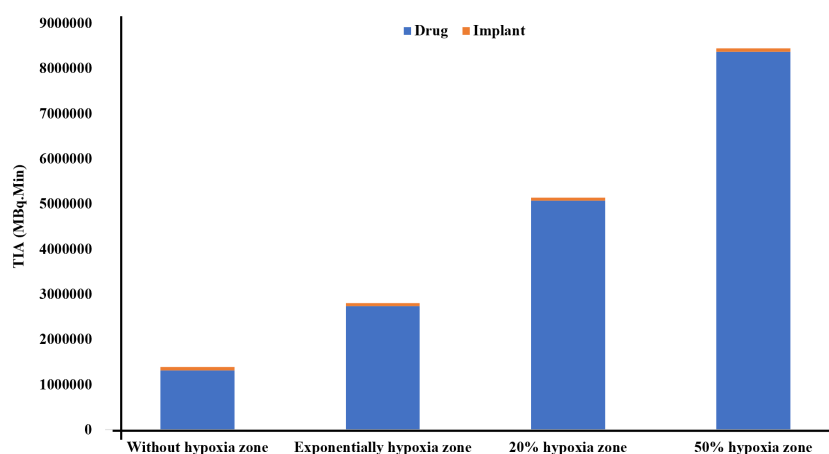


FIGURE 4

Comparison of the TIA [MBq.min] of the radiation source and the drug released from it considering the vascular density and extent of the hypoxia area. It is evident that the radiation source has a significantly lower TIA compared to the released drug. When the tumor experiences 50% hypoxia, TIA of the released drug increases sixfold compared to when there is no hypoxia present.

TABLE 1 Investigated Effect of different combinations of k_{on} and k_{off} on TIA.

KD (k_{off}/k_{on})	K_{on}	K_{off}	TIA _{Drug} [MBq.min]	TIA _{Implant} [MBq.min]
1	0.01	0.01	12.4×10^5	0.69×10^5
1	0.1	0.1	13.5×10^5	
0.1	0.1	0.01	81.04×10^5	
0.1	0.01	0.001	52.2×10^5	
0.01	0.1	0.001	160.7×10^5	
0.01	0.01	0.0001	76.6×10^5	

investigate the influence of K_D on the absorbed dose of ^{177}Lu -PSMA-617. This shared observation suggests that the K_D parameter plays a pivotal role in determining the radiopharmaceutical's concentration, which holds significant implications for the efficacy and therapeutic outcomes of PSMA-targeted therapies.

Furthermore, the results reveal that altering the association rate k_{on} exerts a more pronounced effect compared to adjustments in the dissociation rate k_{off} . As depicted in Figure 7 and Table 1, increasing the association rate k_{on} from 0.01 to 0.1 [L/nmol/min] resulted in a remarkable rise in the TIA from 12.4×10^5 [MBq.min] to 81.04×10^5 [MBq.min], with a fixed dissociation rate k_{off} of 0.01 [1/min]. Based on Figure 7 and Table 1, 6-fold increase in TIA was observed when the dissociation rate k_{off} was changed from 0.01 to 0.0001 (with a fixed association rate k_{on} of 0.01 [L/nmol/min]) (from 12.4×10^5 to 76.6×10^5). It appears from the results that, by reducing the dissociation rate, the drug will have a greater chance of entering the cell, resulting in a higher amount of drug binding and entering

the cell. In addition to the increase in association rate, the drug is able to bind to cell surface receptors faster, which results in less drug being removed from the tumor environment by the blood vessels. Furthermore, the comparison of the TIA of the radiation source also demonstrates that its value is significantly lower than the other results. Even if the drug exhibits different association and dissociation characteristics, leading to varying TIA values, it still outperforms the radiation source.

3.4 Effect of initial amount of ^{177}Lu -PSMA

The initial drug amount loaded into the implant plays a pivotal role in determining treatment efficacy and potential damage to both tumor and surrounding tissues. In this study, varying the initial ^{177}Lu -PSMA-617 amount 7.1×10^7 , 7.1×10^8 , and 7.1×10^9 [Bq] led to distinct responses in terms of survival probability, concentration and damage to normal tissue. The study assumes a condition without hypoxia, with $k_{on}=0.046$ [L/nmol/min] and $k_{off}=0.046$ [1/min] (17). Based on Figures 8 and 9, it is evident that an initial ^{177}Lu -PSMA-617 amount of 7.1×10^9 [Bq] yields the highest total concentration within the tumor. It is important that the amount of radiopharmaceutical used results in maximal damage to the tumor tissue and minimum damage to the normal tissue. For the 7.1×10^7 [Bq] initial radiopharmaceutical amount, the observed percentage of survival probability was 19%, indicating a moderate effect on tumor cell survival (Table 2). However, the impact on normal tissue was relatively low, with TIA calculated at 52×10^{-4} [MBq.min], suggesting minimal harm to healthy cells.

On the contrary, an initial radiopharmaceutical quantity of 7.1×10^8 [Bq] led to an exceptionally low survival probability, approaching nearly zero percent, signifying a robust elimination

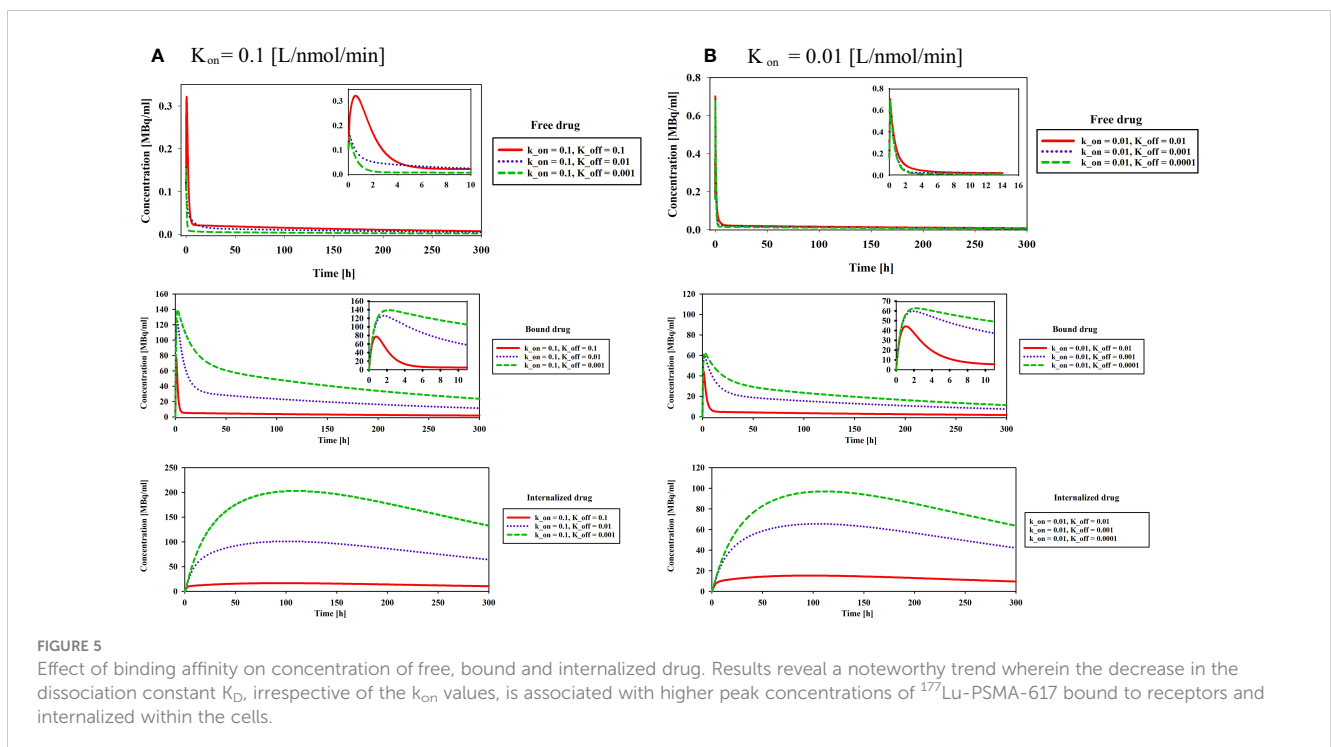


FIGURE 5 Effect of binding affinity on concentration of free, bound and internalized drug. Results reveal a noteworthy trend wherein the decrease in the dissociation constant K_D , irrespective of the k_{on} values, is associated with higher peak concentrations of ^{177}Lu -PSMA-617 bound to receptors and internalized within the cells.

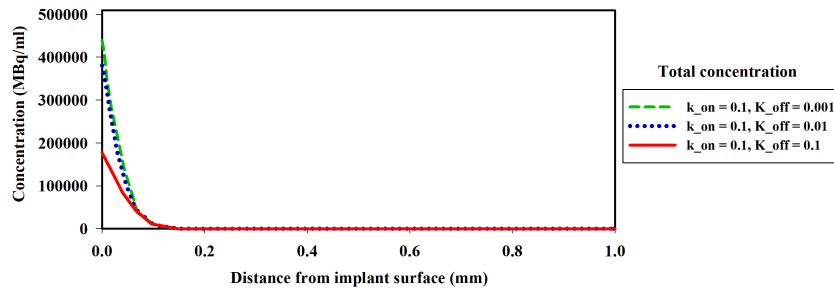


FIGURE 6
The spatial distribution of the concentration of the ¹⁷⁷Lu-PSMA-617 released from the implant around the implant one hour after implantation in the tumor. A decrease in k_D leads to an increase in the total concentration of the drug. The k_{off} variations demonstrate that the highest total concentration is observed at $k_{off}=0.001$ [1/min], indicating enhanced ligand penetration into tumor.

of tumor cells (Table 2). Despite this potent effect on tumor tissue, normal tissues also experienced a higher TIA, with a calculated value of 52×10^{-3} [MBq.min]. This treatment not only exhibited excellent tumor-killing efficacy but also had a slightly increased impact on normal tissue. At the highest initial radiopharmaceutical amount of 7.1×10^9 [Bq], the survival fraction dropped to 0%, illustrating complete eradication of tumor cells (Table 2). However, this extreme effectiveness was accompanied by a higher TIA in normal tissue, calculated at 52×10^{-2} [MBq.min], signifying more significant potential harm to healthy cells.

Overall, these findings underscore the delicate balance required in selecting the initial drug amount for radiopharmaceutical treatment. While higher initial drug amounts demonstrated superior tumor-killing potential, they also showed an elevated impact on normal tissues. The 7.1×10^8 [Bq] initial drug amount exhibited promising outcomes, yielding a considerable TIA within the tumor and notably mitigating harm to normal tissue in contrast to 7.1×10^9 [Bq].

When comparing the effects of the radiation source and the released drug on therapeutic response, considering the initial amount of the drug in the implant shown in Table 2, it becomes

evident that the implant performs poorly as a radiation source in terms of treatment response. Increasing the initial amount of the drug loaded in the implant does improve the TIA and absorbed dose caused by the radiation source. However, these increases, particularly for the values of 7.1×10^7 [Bq] and 7.1×10^8 [Bq], do not result in significant cell death. For instance, with an initial amount of ¹⁷⁷Lu-PSMA at 7.1×10^7 [Bq], the released drug is capable of killing over 80% of cancer cells, while the implant, acting as the radiation source, only contributes 4% to cell death. In summary, these findings highlight the crucial role of drug release and its distribution within the tumor, emphasizing their significant contribution to therapeutic efficacy compared to using the implant solely as a radiation source.

3.5 Analyzing changes in the concentration of a drug

This phase of the investigation is dedicated to scrutinizing the spatial and temporal distribution patterns of radiopharmaceuticals within both the tumor and host tissue. The study operates under a

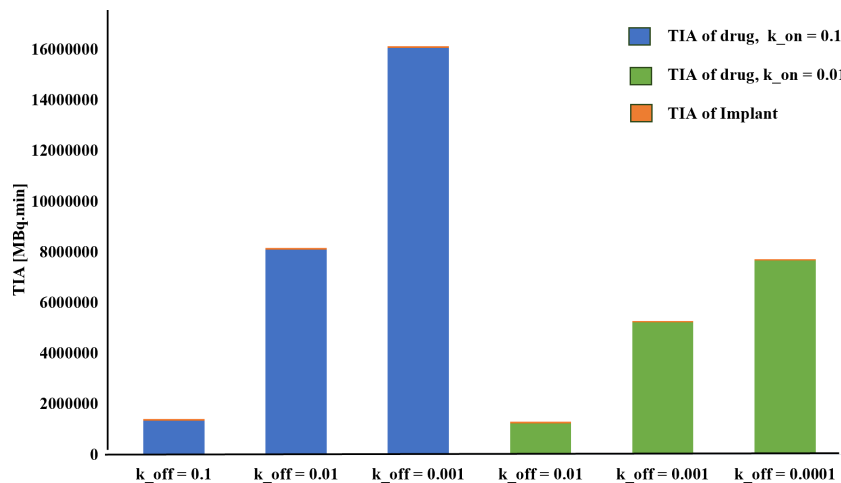


FIGURE 7
TIA comparison for different k_{on} . A higher time-integrated activity (TIA) is observed in the tumor for $k_{on}=0.1$ [L/nmol/min] compared to $k_{on}=0.01$ [L/nmol/min].

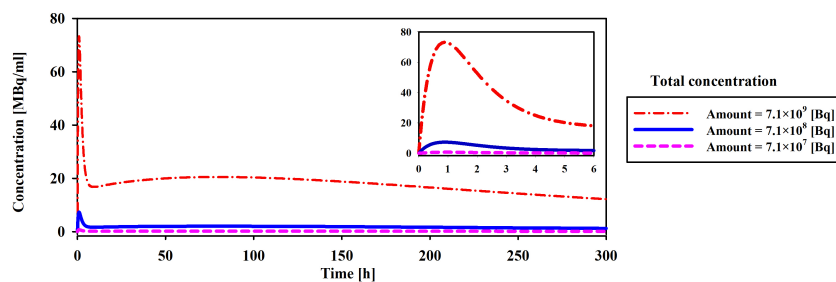


FIGURE 8
 Comparison of total concentration of released drug from the implant for different initial amount of ¹⁷⁷Lu-PSMA. The maximum total concentration in the tumor is achieved when the initial drug amount is set to 7.1×10^9 [Bq].

hypoxia-free condition, characterized by $k_{on}=0.046$ [L/nmol/min] and $k_{off}=0.046$ [1/min] (17), with a loading of 7.1×10^9 [Bq] of ¹⁷⁷Lu-PSMA into the implant. Figure 10 shows drug concentration in the different spaces. When the free radiopharmaceutical enters the interstitial space, it binds to receptors on the cell surface. Radiopharmaceutical initially bind to receptors rapidly. In addition, the lymphatic vessels of normal tissues remove some of the drugs from the interstitial space. Next, the PSMA ligand-protein complex is internalized into the tumor cells via endocytosis. Finally, drugs degrade or are released in cell. The concentrations of bound and free drugs reduce to an undetectable level. As can be seen in Figure 10, the drug concentrations in the tumor are several times higher than in normal tissue in all spaces (Free, Bound, and internalized drugs). Results show that the proposed treatment method has increased drug concentrations in tumors and reduced normal tissue damage. The absorbed dose in tumor was 456 [Gy] (SF in tumor: 0%).

Figure 11 illustrates the spatial distribution of ¹⁷⁷Lu-PSMA within both the tumor and normal tissue at various temporal intervals. The figure distinctly portrays that the maximum Standardized Uptake Value (SUV) is localized within the tumor region, exhibiting values several times higher than those observed in the surrounding normal tissue. The constrained movement of high-molecular-weight PSMA ligands from the implant wall is a pivotal factor in this spatial distribution, contributing positively to minimizing tissue damage surrounding the tumor. It should be

noted that due to the fact that there is no requirement for the radio-drug to enter the cell in order to damage its DNA, the treatment has been effective despite the fact that the drug has not been widely distributed in the tissue.

4 Discussion and conclusion

The use of implants for intratumoral drug delivery represents a promising approach in cancer treatment, offering several advantages over traditional intravenous injection methods (29). Implants allow for localized drug delivery, enabling targeted and sustained release of therapeutic agents directly into the tumor microenvironment (53). This localized drug delivery minimizes systemic exposure and reduces potential side effects, enhancing the overall safety profile of the treatment (54). Moreover, implants can overcome limitations associated with poor drug penetration and distribution within solid tumors, ensuring more efficient drug delivery to cancerous cells. This study presents a novel and comprehensive 3D computational model to simulate the dispersion and localized release of ¹⁷⁷Lu-PSMA-617 after implanting a dual-release system within a solid tumor. The spatial analysis of the results demonstrates that the tumor region exhibits the maximum value of SUV, surpassing the SUV in the surrounding normal tissue by several-fold. The high molecular weight of peptides in PSMA ligands restricts their diffusion from the

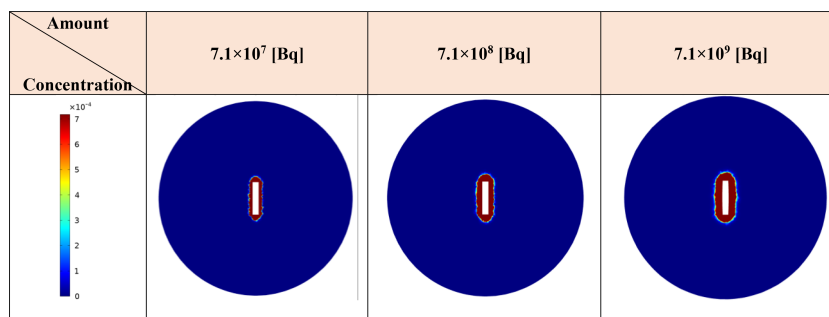


FIGURE 9
 Modifications in the total concentration of released the radiopharmaceutical from implant [MBq/ml] are observed as ¹⁷⁷Lu-PSMA quantity within the implant increases. Elevating the radiopharmaceutical amount results in a greater accumulation of the drug in the vicinity of the implant.

TABLE 2 Effect of amount of ¹⁷⁷Lu-PSMA-617 on TIA.

Amount		7.1×10 ⁷ [Bq]	7.1×10 ⁸ [Bq]	7.1×10 ⁹ [Bq]
Time integrated activity (TIA) [MBq.min]	Released drug in tumor	13 × 10 ³	13 × 10 ⁴	13 × 10 ⁵
	Implant	0.68 × 10 ³	0.68 × 10 ⁴	0.68 × 10 ⁵
Absorbed dose [Gy]	Released drug in tumor	4.56	45.6	456
	Implant	0.23	2.3	23
Survival probability (%)	Released drug in tumor	19%	1.15 × 10 ^{-45%}	0%
	Implant	96%	53%	3 × 10 ^{-14%}
Time integrated activity [MBq.min]	Drug in normal tissue	52 × 10 ⁻⁴	52 × 10 ⁻³	52 × 10 ⁻²

implant wall. Remarkably, this characteristic proves beneficial in limiting tissue damage around the tumor site. The observed 0% survival fraction for the tumor at an activity level of 7.40 MBq highlights the remarkable efficacy of this approach in eradicating tumor cells. Thus, the potential for accurate and successful tumor therapy is shown by this targeted radiopharmaceutical delivery strategy.

The present study seeks to find the effects of hypoxia region extension, binding affinity, and initial drug amount on ¹⁷⁷Lu-PSMA-617 concentration in the tumor microenvironment. In general, the findings of this study demonstrate that elevated hypoxia levels are associated with a higher TIA within tumor due to microvascular density, resulting in enhanced drug availability for

binding to PSMA receptors, reduced clearance of radiopharmaceutical agents from the interstitial space. The 50% hypoxia result in a six-fold increase in TIA within the tumor, relative to non-hypoxic conditions that ultimately promoting greater therapeutic effectiveness.

Another critical aspect under scrutiny is the binding affinity. The results indicate that reducing the dissociation constant (K_D) while keeping k_{on} at 0.1 [L/nmol/min] and varying k_{off} from 0.01 to 0.0001[1/min] results in a substantial 6-fold increase in the TIA. The decrease in K_D and concurrent increase in bound concentration implies a heightened binding affinity of the radiopharmaceutical to the receptors present on the cell surface. Such an elevation in bound and internalized drug concentration results in reduced radiopharmaceutical clearance by vessels, potentially leading to decreased damage to other organs, such as the kidneys.

One of critical parameter under investigation is the initial radiopharmaceutical amount in the implant. This parameter directly influences the total drug concentration available for release and distribution within the tumor. The results allow researchers to determine the optimal amount of drug to be incorporated into the implant, ensuring maximal damage to the tumor while minimizing potential toxicity to surrounding healthy tissues. Among the considered initial radiopharmaceutical amounts of 7.1×10⁷, 7.1×10⁸, and 7.1×10⁹ [Bq], it becomes evident that the 7.1×10⁸ [Bq] amount demonstrates the most advantageous outcomes. Notably, the percentage of survival probability at 7.1×10⁸ [Bq] is significantly lower compared to that at 7.1×10⁷ [Bq], reaching a value of nearly 0%. Furthermore, despite its potent tumor cell elimination capabilities (reflected by the high survival probability), the TIA associated with the 7.1×10⁸ [Bq] amount is one order lower than that of 7.1×10⁹ [Bq], implying a more desirable balance in minimizing adverse effects to normal tissues. Consequently, the initial radiopharmaceutical amount of 7.1×10⁸

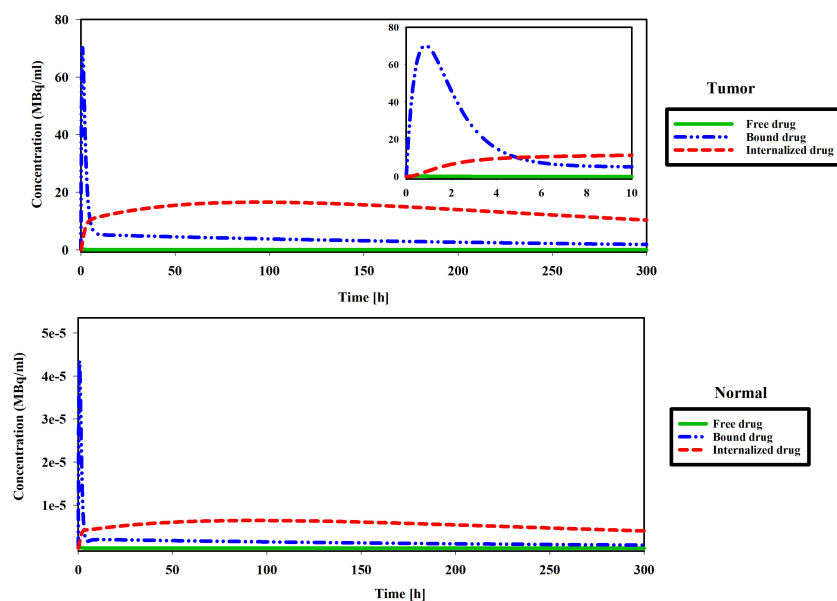


FIGURE 10 Figures show changes in the concentration of free, bound and internalized ¹⁷⁷Lu-PSMA-617 at 300 h.

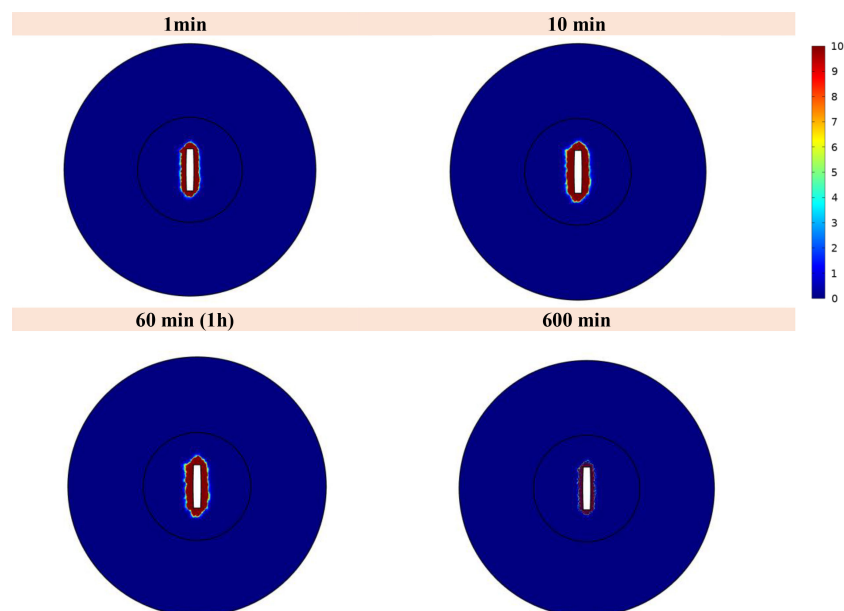


FIGURE 11
Standardized uptake value (SUV) index. The highest SUV is concentrated within the tumor area, displaying values several times greater than those detected in the adjacent normal tissue.

[Bq] stands out as a better choice for achieving therapeutic efficacy while mitigating potential harm to healthy tissues. In our studies, decay of labeled radiopharmaceuticals resulted in relatively negligible unlabeled pharmaceuticals (not shown) that would not pose competition for PSMA binding with radiopharmaceuticals. In addition, it is worth noting that in this study, free PSMA was not taken into consideration due to the local delivery approach. Conversely, when free PSMA is delivered at a high concentration in a small volume, it can lead to receptor saturation on the cell surface, resulting in a diminished therapeutic response. Therefore, by excluding free PSMA in this study, we can ensure that the receptors are not occupied and maximize the potential for an effective therapeutic outcome.

The results obtained from analyzing the TIA in different sections demonstrate that the distribution of radiopharmaceuticals has a more significant therapeutic effect compared to the implant, which also acts as a radiation source. This discrepancy can be attributed to the fact that the radiation source, despite having a high concentration, is only located in the center of the tumor. As a result, only a small portion of the tissue is exposed to radiation. On the other hand, the release of the radiopharmaceutical allows for its penetration into the tissue, resulting in a larger area of tissue being exposed to radiation. These findings highlight the superiority of this treatment approach over brachytherapy. Therefore, utilizing biodegradable implants containing radiopharmaceuticals can offer notable therapeutic performance in comparison to conventional radiotherapy methods.

The experimental design of this study, which revolves around a numerical simulation, is positioned as a pivotal guide for the formulation of optimal drug treatment protocols in future clinical

trials. By delving into the controlled release and dispersion of ^{177}Lu -PSMA through a dual-release implantable delivery system, nuanced insights are garnered into crucial parameters such as hypoxia extension, binding affinity, and initial drug amounts. Through this approach, a more comprehensive understanding of radiopharmaceutical therapy is facilitated, laying the groundwork for the development of meticulously tailored drug treatment strategies. The numerical nature of our study enables a detailed exploration of various dosage scenarios, providing a robust foundation for the optimization of treatment effectiveness in the intricate landscape of the tumor microenvironment. In this manner, the present numerical approach actively shapes the trajectory toward more effective and tailored drug treatments in the clinical trial setting.

In this study, one of limitations is the simplified tumor geometry, chosen based on literature for exploring drug and tumor-related parameters (29). Considering the depth of penetration and tissue distribution, a heterogeneous geometry minimally affects distribution, with only specific areas possibly having higher concentrations. Thus, the choice of simple geometry did not significantly influence the current results. Future studies will employ real tumor geometry for more comprehensive investigations.

Additionally, the utilization of implant-based drug delivery approaches comes with certain limitations. Intratumoral delivery of radiopharmaceuticals is confined to the local area, rendering it incapable of covering the entire body. Consequently, this therapeutic method is more suitable for treating pre-metastatic stages and localized tumors within the body. Moreover, tumors

characterized by extensive angiogenesis present a challenge as the presence of blood vessels can swiftly remove the drug within the interstitial space, hindering effective drug delivery. To ensure optimal performance, it is essential to customize the design of the implant based on the specific characteristics of the tumor tissue. This involves optimizing the loaded capacity, number of inserted implants and release rate of the implant, considering the combined effects of burst and sustained release. By doing so, one can mitigate the risk of undesired outcomes such as elimination by blood/lymphatic microvessels. Overall, the design of the implant should align with the principles of personalized medicine to achieve favorable therapeutic outcomes.

Data availability statement

The original contributions presented in the study are included in the article/Supplementary Material. Further inquiries can be directed to the corresponding author.

Author contributions

AP: Conceptualization, Data curation, Formal Analysis, Investigation, Methodology, Resources, Software, Validation, Visualization, Writing – original draft. MSou: Conceptualization, Data curation, Formal Analysis, Investigation, Software, Validation, Writing – review & editing. AR: Data curation, Funding acquisition, Resources, Writing – review & editing. MSol: Project administration, Resources, Supervision, Writing – review & editing.

References

1. Rawla P. Epidemiology of prostate cancer. *World J Oncol.* (2019) 10:63. doi: 10.14740/wjon1191.
2. Zhao J, Xu H, Su Y, Pan J, Xie S, Xu J, et al. Emerging regulatory mechanisms of n6-methyladenosine modification in cancer metastasis. *Phenomics.* (2023) 3:83–100. doi: 10.1007/s43657-021-00043-w.
3. James SS, Bednarz B, Benedict S, Buchsbaum JC, Dewaraja Y, Frey E, et al. Current status of radiopharmaceutical therapy. *Int J Radiat Oncol Biol Phys.* (2021) 109:891–901. doi: 10.1016/j.ijrobp.2020.08.035.
4. Achard V, Putora PM, Omlin A, Zilli T, Fischer S. Metastatic prostate cancer: treatment options. *Oncology.* (2022) 100:48–59. doi: 10.1159/000519861.
5. Posdzich P, Darr C, Hilsner T, Wahl M, Herrmann K, Hadaschik B, et al. Metastatic prostate cancer—A review of current treatment options and promising new approaches. *Cancers.* (2023) 15:461. doi: 10.3390/cancers15020461.
6. Sgouros G, Bodei L, McDevitt MR, Nedrow JR. Radiopharmaceutical therapy in cancer: clinical advances and challenges. *Nat Rev Drug discovery.* (2020) 19:589–608. doi: 10.1038/s41573-020-0073-9.
7. Kashkooli FM, Soltani M, Souri M. Controlled anti-cancer drug release through advanced nano-drug delivery systems: Static and dynamic targeting strategies. *J Controlled release.* (2020) 327:316–49. doi: 10.1016/j.jconrel.2020.08.012.
8. Vallabhajosula S. *Molecular Imaging and Targeted Therapy: Radiopharmaceuticals and Clinical Applications.* Springer Nature, Switzerland (2023). doi: 10.1007/978-3-031-23205-3.
9. Kiani Shahvandi M, Soltani M, Moradi Kashkooli F, Saboury B, Rahmim A. Spatiotemporal multi-scale modeling of radiopharmaceutical distributions in vascularized solid tumors. *Sci Rep.* (2022) 12:14582. doi: 10.1038/s41598-022-18723-6.
10. Tian M, Zuo C, Civelek AC, Carrio I, Watanabe Y, Kang KW, et al. International nuclear medicine consensus on the clinical use of amyloid positron emission tomography in Alzheimer's disease. *Phenomics.* (2023) 3:375–89. doi: 10.1007/s43657-022-00068-9.
11. Salih S, Alkhatheeri A, Alomaim W, Elliyanti A. Radiopharmaceutical treatments for cancer therapy, radionuclides characteristics, applications, and challenges. *Molecules.* (2022) 27:5231. doi: 10.3390/molecules27165231.
12. O'Neill E, Mosley M, Cornelissen B. Imaging DNA damage response by γ H2AX *in vivo* predicts treatment response to Lutetium-177 radioligand therapy and suggests senescence as a therapeutically desirable outcome. *Theranostics.* (2023) 13:1302. doi: 10.7150/thno.82101
13. Nguyen CB, Alva AS. The future of radioligand therapies in metastatic castrate-resistant prostate cancer. *Adv Oncol.* (2023) 3(1):129–36. doi: 10.1016/j.yao.2023.01.009.
14. Piranfar A, Soltani M, Kashkooli FM, Uribe CF, Rahmim A. Spatiotemporal modeling of radiopharmaceutical transport in solid tumors: application to ^{177}Lu -PSMA therapy of prostate cancer. *Comput Methods Programs Biomed.* (2024) 108004. doi: 10.1016/j.cmpb.2023.108004.
15. Jang A, Kendi AT, Sartor O. Status of PSMA-targeted radioligand therapy in prostate cancer: current data and future trials. *Ther Adv Med Oncol.* (2023) 15:17588359231157632. doi: 10.1177/17588359231157632.
16. Handkiewicz-Junak D, Poeppel TD, Bodei L, Aktolun C, Ezziddin S, Giammarile F, et al. EANM guidelines for radionuclide therapy of bone metastases with beta-emitting radionuclides. *Eur J Nucl Med Mol imaging.* (2018) 45:846–59. doi: 10.1007/s00259-018-3947-x.
17. Kletting P, Schuchardt C, Kulkarni HR, Shahinfar M, Singh A, Glatting G, et al. Investigating the effect of ligand amount and injected therapeutic activity: a simulation study for ^{177}Lu -labeled PSMA-targeting peptides. *PLoS One.* (2016) 11:e0162303. doi: 10.1371/journal.pone.0162303.

Funding

The author(s) declare financial support was received for the research, authorship, and/or publication of this article. The authors acknowledge funding in part by the Canadian Institutes of Health Research (CIHR) Project Grant PJT-162216.

Conflict of interest

The authors declare that the research was conducted in the absence of any commercial or financial relationships that could be construed as a potential conflict of interest.

Publisher's note

All claims expressed in this article are solely those of the authors and do not necessarily represent those of their affiliated organizations, or those of the publisher, the editors and the reviewers. Any product that may be evaluated in this article, or claim that may be made by its manufacturer, is not guaranteed or endorsed by the publisher.

Supplementary material

The Supplementary Material for this article can be found online at: <https://www.frontiersin.org/articles/10.3389/fonc.2024.1320371/full#supplementary-material>

18. Sgouros G. Radiopharmaceutical therapy. *Health physics*. (2019) 116:175. doi: 10.1097/HP.0000000000001000.
19. Shahvandi MK, Souri M, Tavasoli S, Kashkooli FM, Kar S, Soltani M. A comparative study between conventional chemotherapy and photothermal activated nano-sized targeted drug delivery to solid tumor. *Comput Biol Med*. (2023) 166:107574. doi: 10.1016/j.compbio.2023.107574.
20. Abuqbeitah M, Demir M, Uslu-Bešli L, Yeyin N, Sönmezöglü K. Blood clearance and occupational exposure for 177 Lu-DOTATATE compared to 177 Lu-PSMA radionuclide therapy. *Radiat Environ Biophys*. (2018) 57:55–61. doi: 10.1007/s00411-017-0721-6.
21. Park EA, Graves SA, Menda Y. The impact of radiopharmaceutical therapy on renal function. *Semin Nucl Med*. (2022) 52(4):467–474. doi: 10.1053/j.semnuclmed.2022.02.004.
22. Park S, Kim J, Lee C. Injectable rapidly dissolving needle-type gelatin implant capable of delivering high concentrations of H₂O₂ through intratumoral injection. *Biomed Pharmacother*. (2022) 156:113910. doi: 10.1016/j.biopha.2022.113910.
23. Souri M, Soltani M, Kashkooli FM, Shahvandi MK, Chiani M, Shariati FS, et al. Towards principled design of cancer nanomedicine to accelerate clinical translation. *Materials Today Bio*. (2022), 13:100208. doi: 10.1016/j.mtbo.2022.100208.
24. Souri M, Soltani M, Kashkooli FM, Shahvandi MK. Engineered strategies to enhance tumor penetration of drug-loaded nanoparticles. *J Controlled Release*. (2022) 341:227–46. doi: 10.1016/j.jconrel.2021.11.024.
25. Wilhelm S, Tavares AJ, Dai Q, Ohta S, Audet J, Dvorak HF, et al. Analysis of nanoparticle delivery to tumours. *Nat Rev materials*. (2016) 1:1–12. doi: 10.1038/natrevmats.2016.14.
26. Golombok SK, May J-N, Theek B, Appold L, Drude N, Kiessling F, et al. Tumor targeting via EPR: Strategies to enhance patient responses. *Advanced Drug Delivery Rev*. (2018) 130:17–38. doi: 10.1016/j.addr.2018.07.007.
27. Izci M, Maksoudian C, Manshian BB, Soenen SJ. The use of alternative strategies for enhanced nanoparticle delivery to solid tumors. *Chem Rev*. (2021) 121:1746–803. doi: 10.1021/acs.chemrev.0c00779.
28. Souri M, Soltani M, Moradi Kashkooli F. Computational modeling of thermal combination therapies by magneto-ultrasonic heating to enhance drug delivery to solid tumors. *Sci Rep*. (2021) 11:19539. doi: 10.1038/s41598-021-98554-z.
29. Al-Zu'bi M, Mohan A. Modelling of combination therapy using implantable anticancer drug delivery with thermal ablation in solid tumor. *Sci Rep*. (2020) 10:19366. doi: 10.1038/s41598-020-76123-0.
30. Chua CYX, Ho J, Demaria S, Ferrari M, Grattoni A. Emerging technologies for local cancer treatment. *Advanced Ther*. (2020) 3:2000027. doi: 10.1002/adtp.202000027.
31. Groh CM, Hubbard ME, Jones PF, Loadman PM, Periasamy N, Sleeman BD, et al. Mathematical and computational models of drug transport in tumours. *J R Soc Interface*. (2014) 11:20131173. doi: 10.1098/rsif.2013.1173.
32. Kashkooli FM, Soltani M, Souri M, Meaney C, Kohandel M. Nexus between *in silico* and *in vivo* models to enhance clinical translation of nanomedicine. *Nano Today*. (2021) 36:101057. doi: 10.1016/j.nantod.2020.101057.
33. Souri M, Kiani Shahvandi M, Chiani M, Moradi Kashkooli F, Farhangi A, Mehrabi MR, et al. Stimuli-sensitive nano-drug delivery with programmable size changes to enhance accumulation of therapeutic agents in tumors. *Drug Delivery*. (2023) 30:2186312. doi: 10.1080/10717544.2023.2186312.
34. Solorio L, Patel RB, Wu H, Krupka T, Exner AA. Advances in image-guided intratumoral drug delivery techniques. *Ther delivery*. (2010) 1:307–22. doi: 10.4155/tde.10.20.
35. Moradi Kashkooli F, Souri M, Tavakkoli J, C. Kolios M. A spatiotemporal computational model of focused ultrasound heat-induced nano-sized drug delivery system in solid tumors. *Drug Delivery*. (2023) 30:2219871. doi: 10.1080/10717544.2023.2219871.
36. Soltani M, Chen P. Numerical modeling of fluid flow in solid tumors. *PLoS One*. (2011) 6:e20344. doi: 10.1371/journal.pone.0020344.
37. Kashkooli FM, Abazari MA, Soltani M, Ghazani MA, Rahmim A. A spatiotemporal multi-scale computational model for FDG PET imaging at different stages of tumor growth and angiogenesis. *Sci Rep*. (2022) 12:10062. doi: 10.1038/s41598-022-13345-4.
38. O'Donoghue J, Zanzonico P, Humm J, Kesner A. Dosimetry in radiopharmaceutical therapy. *J Nucl Med*. (2022) 63:1467–74. doi: 10.2967/jnumed.121.262305.
39. Hindorf C. *Internal dosimetry. Chapter 18*(2014).
40. Begum NJ, Thieme A, Eberhardt N, Tauber R, D'Alessandria C, Beer AJ, et al. The effect of total tumor volume on the biologically effective dose to tumor and kidneys for 177Lu-labeled PSMA peptides. *J Nucl Med*. (2018) 59:929–33. doi: 10.2967/jnumed.117.203505.
41. Spoomans K, Crabbé M, Struelens L, De Saint-Hubert M, Koole M. A review on tumor control probability (TCP) and preclinical dosimetry in targeted radionuclide therapy (TRT). *Pharmaceutics*. (2022) 14:2007. doi: 10.3390/pharmaceutics14102007.
42. Birindelli G, Drobnjakovic M, Morath V, Steiger K, D'Alessandria C, Gourni E, et al. Is hypoxia a factor influencing PSMA-directed radioligand therapy?—An *in silico* study on the role of chronic hypoxia in prostate cancer. *Cancers*. (2021) 13:3429. doi: 10.3390/cancers13143429.
43. Stylianopoulos T, Munn LL, Jain RK. Reengineering the physical microenvironment of tumors to improve drug delivery and efficacy: from mathematical modeling to bench to bedside. *Trends cancer*. (2018) 4:292–319. doi: 10.1016/j.trecan.2018.02.005.
44. Raghunathan S, Evans D, Sparks JL. Poroviscoelastic modeling of liver biomechanical response in unconfined compression. *Ann Biomed engineering*. (2010) 38:1789–800. doi: 10.1007/s10439-010-9957-x.
45. Boucher Y, Jain RK. Microvascular pressure is the principal driving force for interstitial hypertension in solid tumors: implications for vascular collapse. *Cancer Res*. (1992) 52:5110–4.
46. Kashkooli FM, Soltani M, Rezaeian M, Meaney C, Hamed M-H, Kohandel M. Effect of vascular normalization on drug delivery to different stages of tumor progression: *In-silico* analysis. *J Drug Delivery Sci Technol*. (2020) 60:101989. doi: 10.1016/j.jddst.2020.101989.
47. Zhan W, Gedroyc W, Xu XY. The effect of tumour size on drug transport and uptake in 3-D tumour models reconstructed from magnetic resonance images. *PLoS One*. (2017) 12:e0172276. doi: 10.1371/journal.pone.0172276.
48. Zhang W, Fan W, Rachagani S, Zhou Z, Lele SM, Batra SK, et al. Comparative study of subcutaneous and orthotopic mouse models of prostate cancer: vascular perfusion, vasculature density, hypoxic burden and BB2r-targeting efficacy. *Sci Rep*. (2019) 9:11177. doi: 10.1038/s41598-019-47308-z.
49. Souri M, Moradi Kashkooli F, Soltani M. Analysis of magneto-hyperthermia duration in nano-sized drug delivery system to solid tumors using intravascular-triggered thermosensitive-liposome. *Pharm Res*. (2022) 39:753–65. doi: 10.1007/s11095-022-03255-5.
50. Soltani M, Souri M, Moradi Kashkooli F. Effects of hypoxia and nanocarrier size on pH-responsive nano-delivery system to solid tumors. *Sci Rep*. (2021) 11:19350. doi: 10.1038/s41598-021-98638-w.
51. Begum NJ, Glatting G, Wester H-J, Eiber M, Beer AJ, Kletting P. The effect of ligand amount, affinity and internalization on PSMA-targeted imaging and therapy: A simulation study using a PBPK model. *Sci Rep*. (2019) 9:20041. doi: 10.1038/s41598-019-56603-8.
52. Pan AC, Borhani DW, Dror RO, Shaw DE. Molecular determinants of drug-receptor binding kinetics. *Drug Discovery Today*. (2013) 18:667–73. doi: 10.1016/j.drudis.2013.02.007.
53. De Souza R, Zahedi P, Allen CJ, Piquette-Miller M. Polymeric drug delivery systems for localized cancer chemotherapy. *Drug delivery*. (2010) 17:365–75. doi: 10.3109/10717541003762854.
54. Pial MMH, Tomitaka A, Pala N, Roy U. Implantable devices for the treatment of breast cancer. *J Nanotheranostics*. (2022) 3:19–38. doi: 10.3390/jnt3010003.